Structure and dynamics of repulsive magnetorheological colloids in two-dimensional channels

Ramin Haghgooie and Patrick S. Doyle*
Department of Chemical Engineering, Massachusetts Institute of Technology, Cambridge, Massachusetts 02139, USA
(Received 31 January 2005; revised manuscript received 7 May 2005; published 19 July 2005)

We study a system of colloidal spheres with induced magnetic dipoles confined in two-dimensional (2D) hard-wall channels using Brownian dynamics simulations. The external magnetic field is directed normal to the 2D plane and therefore the colloids interact with a purely repulsive r^{-3} potential. The effects of confinement between parallel walls are determined by analyzing the structure and dynamics of these confined systems and comparing to the unbounded (infinite) 2D plane limit. The bond-order correlation function is analyzed as a function of time and exhibits unique characteristics associated with the channel-like confinement. The existence of a plateau in this correlation function is observed over an intermediate time scale and the fate of the plateau (decay or persistence) depends upon the channel width, the strength of the external magnetic field, and the number density. The plateau is analyzed in further detail and an explanation is put forth for its existence and subsequent long time behavior. Additionally, re-entrant behavior with respect to dimensionless channel width is observed in the structural properties and an associated state-diagram is presented for these systems.

DOI: 10.1103/PhysRevE.72.011405 PACS number(s): 82.70.Dd, 61.72.−y, 75.40.Mg, 64.60.Cn

I. INTRODUCTION

Magnetorheological (MR) fluids are suspensions of colloids which acquire dipole moments under application of a magnetic field. Recently there has been much interest in using the colloids in these fluids as structural components in microfluidic applications. There have been a number of studies on confined systems of MR fluids in recent years ranging from determination of fundamental properties of the self-assembly to applications utilizing the self-assembled structures. Self-assembly of MR fluids in the thin slit geometry has been well studied and the types of structures that form in this geometry have been characterized [1–3]. At low volume fractions, the MR fluid self-assembles into a structure characterized by uniformly spaced columns that span the height of the slit [1]. Using more complex fields such as a rotating field, periodic planar structures have been observed in the plane of the rotating field between parallel walls [2]. At higher volume fractions, in thin slits, more complex structures can be formed that are highly dependent upon the thickness of the slit [3].

Researchers have begun to take advantage of the unique combination of structural and dynamical capabilities that MR fluids offer in order to design microdevices utilizing these properties. Experimental studies have been performed on a variety of applications involving self-assembled MR fluids in confined geometries [4–9]. Of particular interest is the use of these MR colloids as structural components for biomolecule separation devices. The porous network of columns formed by MR fluids in microfluidic channels has been shown to be effective for size dependent separation of DNA [4,5].

In this work we present an analysis of the dynamics of equilibrium structures created by the self-assembly of MR fluids in two-dimensional (2D) channels and show how those dynamics are correlated with the structure. Self-assembly of field-responsive colloids in 2D has been widely studied because it is a model system with very interesting physics. The most studied aspect of these systems is the nature of the solid-liquid phase transition. In the unbounded (infinite plane) 2D system, it has been theorized that the nature of the solid-liquid phase transition is second order with an intermediate stable hexatic phase [10–12]. There is compelling experimental evidence supporting the existence of a hexatic phase in the case of purely repulsive dipoles [13–15]. While many simulation studies have been performed upon a variety of 2D colloidal systems, the nature of the phase transition has not yet been conclusively determined in simulations [16–21].

In addition to the nature of the phase transition, many researchers have been interested in the properties of 2D colloids confined laterally. Much of this research has focused on circular confinements [22–27]. This confinement imposes a circular shell-like structure upon the crystal and leads to very unique properties of the phase transition. Nonhomogeneous melting has been observed in these systems where the melting begins at the boundary between the shell-like structure and the more hexagonal structure in the center of the circular confinement [23,24]. Additionally, re-entrant freezing was observed in small clusters of colloids confined in 2D circles due to radial fluctuations [22,25,26]. As the interaction strength between the colloids was decreased the clusters transitioned from solidlike to liquidlike. However as the interaction strength was further decreased, increased radial fluctuations of the colloids caused rings of colloids to become locked in register with one another and produced re-entrant freezing behavior. This type of re-entrant phase behavior was also observed in systems of 2D colloids confined in periodic 1D light fields [28–30].

Another very important form of constraint for 2D colloidal systems is channel-like confinement. This type of system has the obvious application towards studying microfluidic geometries. Additionally, channel-like confinement breaks the symmetry that exists in circular confinements leading to different structures and dynamics. A few experimental stud-

*Electronic address: pdoyle@mit.edu

ies have been done on colloidal-like systems confined in quasi-2D channels [31–33]. Teng *et al.* [31] observed anisotropic diffusion, enhanced in the direction parallel to the confining walls when studying a dusty plasma system confined in a quasi-2D channel. The other studies were performed on spherical block copolymers confined in a 2D channel [32,33] and the authors observed that the orientational order decayed in the regions farther from the wall. Recently, simulation and theory have been performed on a system of colloids in narrow 2D channels interacting with a Yukawa potential [34]. The channel walls in these studies consisted of a parabolic confining potential. The authors observed re-entrant behavior as a function of the density of colloids in the channels and they characterized the structural and melting transitions that occur in this system.

We have recently presented a simulation study on repulsive dipoles confined in 2D channels and have fully characterized the types of structures that form in these systems [35]. Here we will present an analysis of the dynamics in these systems and demonstrate the close connection between the structure and dynamics that are observed. The organization of this paper is as follows. In Sec. II we present the details for the simulations performed in this study. In Sec. III we present our results for the simulations of the unbounded 2D system. We then compare those results to 2D channel systems in Sec. IV. In Sec. IV A we discuss in further detail the interesting dynamics that we have observed in the channel systems. We illustrate the link between structure and dynamics in Sec. IV B. Combining all of the results, we present a state-diagram for these 2D systems in Sec. V. We discuss the generality of the state-diagram in Sec. VI and in Sec. VII we summarize our findings and discuss the impact of this work.

II. SIMULATION DETAILS

The system studied consisted of MR colloids confined to a 2D plane with a uniform external magnetic field directed normal to the confining plane. The details of the simulations are given in a recent publication [35] and we summarize here the major points. In this system, the colloids interact with a purely repulsive dipolar potential. We have modeled the MR colloids as hard spheres with repulsive point dipoles at their centers. This approach has been used widely in the literature [35–37] and has been shown to be a good approximation for the magnetic behavior of MR colloids [38]. The large separation distances between the colloids in this system ensure that the dominant magnetic field is the external field and the effect of mutual induction between colloids is negligible. The pairwise dipolar interaction energy (V_{ij}) is given by

$$V_{ij}(r_{ij}) = \epsilon\left(\frac{d}{r_{ij}}\right)^3, \tag{1}$$

where $\epsilon = \mu_o M(B)^2/4\pi d^3$ is the energy scale and d is the diameter of the hard sphere. The center-to-center distance between the two colloids i and j is given by r_{ij}, μ_o is the magnetic permeability of free space, and $M(B)$ is the dipole moment of an individual colloid and is a function of the magnetic field strength (B). A dimensionless field strength is then defined as

$$\Gamma = \frac{\epsilon}{k_B T}\left(\frac{d}{R}\right)^3, \tag{2}$$

where R is defined as $R = a \sin 60$ and a is the lattice spacing in a perfectly hexagonal 2D crystal. The lattice spacing is a purely geometric property and is a function of the number density in the system (n) such that $a = (n\sqrt{3}/2)^{-1/2}$. The number density is defined as the number of colloids in the system divided by the total area available to the centers of the colloids. Therefore, the length scale in terms of the number density in the system is written as

$$R = \left(\frac{2}{\sqrt{3}n}\right)^{-1/2}. \tag{3}$$

The dimensionless interaction energy in the system is thus defined as

$$\frac{V_{ij}(r_{ij})}{k_B T} = \Gamma\left(\frac{R}{r_{ij}}\right)^3, \tag{4}$$

resulting in the interesting observation that all 2D dipolar systems at the same Γ behave identically, as long as R is the only relevant length scale in the system (i.e., $d \ll R$) [37] as is the case for all of the results reported here.

Brownian dynamics simulations were used to study this system [39]. The equation of motion is approximated by the stochastic differential equation

$$d\mathbf{r}_i(t) \simeq \frac{1}{\zeta}\mathbf{F}_{s,i}(\mathbf{r}_j(t))dt + \sqrt{\frac{2k_B T}{\zeta}}d\mathbf{W}_i, \tag{5}$$

where the inertia of the colloids is neglected. The parameter $\mathbf{W}_i$ is a Wiener process with $\langle d\mathbf{W}_i \rangle = 0$ and $\langle d\mathbf{W}_i d\mathbf{W}_j \rangle = dt\boldsymbol{\delta}$ where $\boldsymbol{\delta}$ is the identity tensor. This Wiener process represents the thermal fluctuations in the system. $\mathbf{F}_{s,i}(\mathbf{r}_j(t))$ is the sum of all pairwise interactions in the system including dipole-dipole interactions and ζ is the drag coefficient on a single colloid. For simplicity, we neglect hydrodynamic interactions. The equation of motion was integrated forward in time using an Euler integration. At the end of a time step, hard sphere overlaps were treated by displacing overlapped colloids along the line connecting their centers until they are just contacting [40]. In this manner, we project out any unphysical moves that may occur during the course of a time step. This procedure was performed for all overlaps, between two colloids and between colloids and hard walls, and was iterated until all overlaps in the system were removed. Due to the large magnitude of the repulsive interactions compared to the thermal motion in our 2D systems (at the field strengths we simulated) we never observed overlaps between colloids, only overlaps between the colloids and the walls.

Simulations of the unbounded system were performed with 14 784 colloids. We imposed periodic boundary conditions in the x and y directions and the magnetic field was aligned in the z direction. Simulations of the channel systems were done with 960–3840 colloids. In these systems we imposed periodic boundary conditions in the y direction and

hard walls in the x direction. A time step of $\tilde{dt}=7.5\times10^{-5}$ was used where time is made dimensionless as $\tilde{t}=tk_BT/\zeta R^2$. The time necessary for a colloid to freely diffuse a unit distance R is given by $\zeta R^2/k_BT$. A cutoff for the dipole-dipole interaction of $6.5R$ was used along with a linked-list binning algorithm [41] where the bin sizes were slightly larger than the cutoff value. Therefore, only interactions between colloids separated by a distance less than the cutoff were considered.

The number density in the simulations reported here was held constant at $n=0.0462$ such that $d \ll R$. For the channel systems, the width of the channel was taken to be the width accessible to the centers of the colloids. This definition implies that the width of the channel used for calculating the number density is in fact the true width of the channel minus d. Defining the channel width in this way ensures that we remove any system dependence on the colloid diameter d. In the unbounded systems the area is simply the true area since we have periodic boundary conditions in all directions. All of the simulations were determined to be converged in system size, time step, and cutoff for the dipole-dipole interaction.

III. UNBOUNDED 2D SYSTEM

The unbounded systems were equilibrated from a perfect hexagonal lattice. The total defect concentration was tracked as a function of time and the system was determined to be at equilibrium when the defect concentration ($C_{\mathrm{def}}^{\mathrm{b}}$) remained unchanged over a dimensionless time of 373. A defect is defined as a colloid with more or less than six nearest neighbors. Statistics were taken after the system was determined to be equilibrated. Examples of the equilibration curves are shown in Fig. 1(a). In the liquid phase, near the transition field strength, the equilibration was slower than for systems farther away from the phase boundary. This is shown in Fig. 1(a) where the equilibration of the unbounded system at a dimensionless field strength of 12.41 is much faster than at a dimensionless field strength of 14.89. Fluctuations in the defect concentration also increase near the phase boundary which is consistent with the recent work of Reichhardt and Reichhardt [42]. The state of the unbounded system was determined by calculating the bond-order correlation function in time ($g_6(\tilde{\tau})$) [43]. The correlation function is given by the equation

$$g_6(\tilde{\tau}) = \langle \Psi_6^*(0)\Psi_6(\tilde{\tau})\rangle, \tag{6}$$

where $\tilde{\tau}$ is the dimensionless lag time and Ψ_6 is the local bond order parameter

$$\Psi_6 = \frac{1}{m}\sum_{k=1}^{m} e^{i6\theta_k}. \tag{7}$$

In Eq. (7), m is the number of nearest neighbors for a given colloid and θ_k is the angle between the vector connecting the colloid and its kth nearest neighbor and an arbitrary reference axis. The nearest neighbors are determined by performing a Delaunay triangulation. Theory predicts that the behavior of $g_6(\tilde{\tau})$ in time can be used to determine the phase of the unbounded system [43]. In the solid phase, $g_6(\tilde{\tau})$ remains constant for all lag times while in the liquid phase $g_6(\tilde{\tau})$ decays exponentially to zero as a function of lag time. In the hexatic phase, $g_6(\tilde{\tau})$ decays algebraically to zero as a function of lag time. The bond-order correlation function is plotted in Fig. 1(b) for a variety of dimensionless field strengths. We were able to equilibrate the liquid phase up to a dimensionless field strength of 14.89 and the solid phase down to a dimensionless field strength of 15.2. Between these two field strengths we were not able to converge our unbounded system due to the diverging correlation lengths and times near the phase transition [44] and therefore we are not able to comment upon the existence of a hexatic phase in this system. However, our results clearly indicate that the solid-liquid phase transition occurs between a dimensionless field strength of 14.89 and 15.2. This range is in good agreement with the simulation results of Löwen [45] for the same type of system. However, Löwen used an empirical criterion to determine the transition point and the system size was much smaller ($N=961$) than the current study. Experimental studies have shown the existence of a hexatic phase between a dimensionless field strength of 12.14 and 13.93 with a liquid phase below 12.14 and a solid phase above 13.93 [13], a slightly lower range than our simulation results. However, our determination of the phase boundary region in the unbounded system serves as a base case for our simulation study which we will perturb by introducing parallel walls into our 2D system.

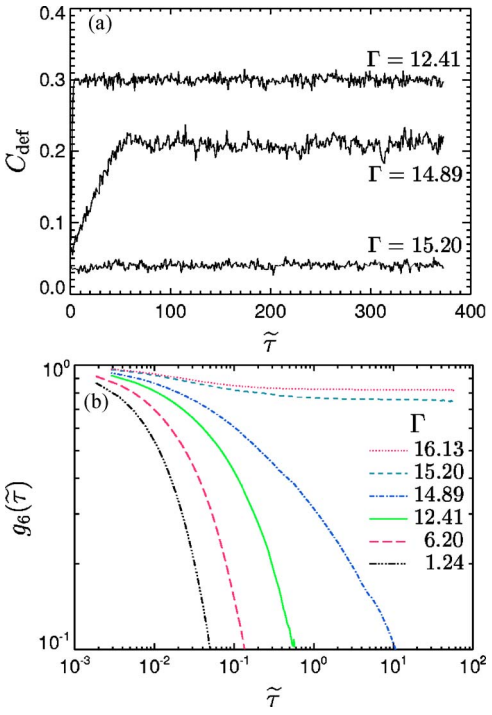

FIG. 1. (Color online) (a) Defect concentration as a function of time during the equilibration of the unbounded system at three dimensionless field strengths. (b) The bond-order correlation function for unbounded 2D systems at several dimensionless field strengths. Above a dimensionless field strength of 15.20 the system behaves as a solid crystal and below a dimensionless field strength of 14.89 the system behaves as a liquid.

IV. 2D CHANNELS

Each channel system was annealed from a liquid state to the desired dimensionless field strength. The concentration of defects in the channel was tracked as a function of time to determine when equilibrium had been reached. We assumed the system was sufficiently equilibrated when the concentration of defects did not change over a time period of 373. Statistics were taken thereafter. Previously we characterized the equilibrium structures that form in these systems and we found that the colloids along the walls exhibit significantly different behavior from the colloids in the bulk [35]. We performed an analysis of the dynamics of the colloids against the wall and found that they are highly localized and remain so over the duration of our simulations. Therefore, in this work we will focus on the dynamics of the bulk colloids. A bulk colloid is defined as any colloid located at a distance greater than $R/2$ from the wall. *All of the results presented for $g_6(\tilde{\tau})$ are given for the bulk colloids only.*

The bond-order correlation function is shown in Fig. 2 for a variety of channel widths at two different field strengths. In Fig. 2(a), $g_6(\tilde{\tau})$ is shown for channels at a dimensionless field strength of 16.13, a value well into the solid phase for an unbounded system. For a channel width of 100, the $g_6(\tilde{\tau})$ behavior is indistinguishable from the behavior in the unbounded system showing that the channel system approaches the unbounded system in the limit of large channels. As the channel width is made narrower the channel system becomes more disordered than the unbounded system at this dimensionless field strength [35]. This trend towards more disorder is nonmonotonic and exhibits several oscillations as a function of channel width. An example of these oscillations is illustrated by the $g_6(\tilde{\tau})$ behavior for the dimensionless channel widths 5–3 (g–a) in Fig. 2(a).

In Fig. 2(b), $g_6(\tilde{\tau})$ is shown for channels at a dimensionless field strength of 12.41. This field strength is well into the liquid phase in the unbounded system where $g_6(\tilde{\tau})$ decays exponentially to zero. In Fig. 2(b) [and Fig. 2(c)] at a channel width of 100, the $g_6(\tilde{\tau})$ curve begins to decay exponentially and is indistinguishable from the unbounded curve. However, at a dimensionless lag time of ~ 1, a plateau begins to develop and the curve deviates from the unbounded case. Eventually at a dimensionless lag time of ~ 50 the plateau begins to decay exponentially again. We will discuss this plateau in more detail in Sec. IV A. As the channel width is made narrower the channel system becomes more ordered than the unbounded system at this field strength. Again, the nonmonotonic behavior in $g_6(\tilde{\tau})$ is observed for this dimensionless field strength. In Fig. 2(b) oscillations are shown for dimensionless channel widths 5–3 (g–a). However, in general as the channel width becomes wider the unbounded case is approached slowly as seen in Fig. 2(c), where four $g_6(\tilde{\tau})$ curves are shown for successively wider channels, 10, 20, 50, and 100 at a dimensionless field strength of 12.41. The second exponential decay of the plateau only becomes evident for channels with a channel width $\tilde{w} \geq 20$. The existence of this intermediate time plateau is a very interesting feature of this system and we offer below an explanation for its origin and subsequent decay.

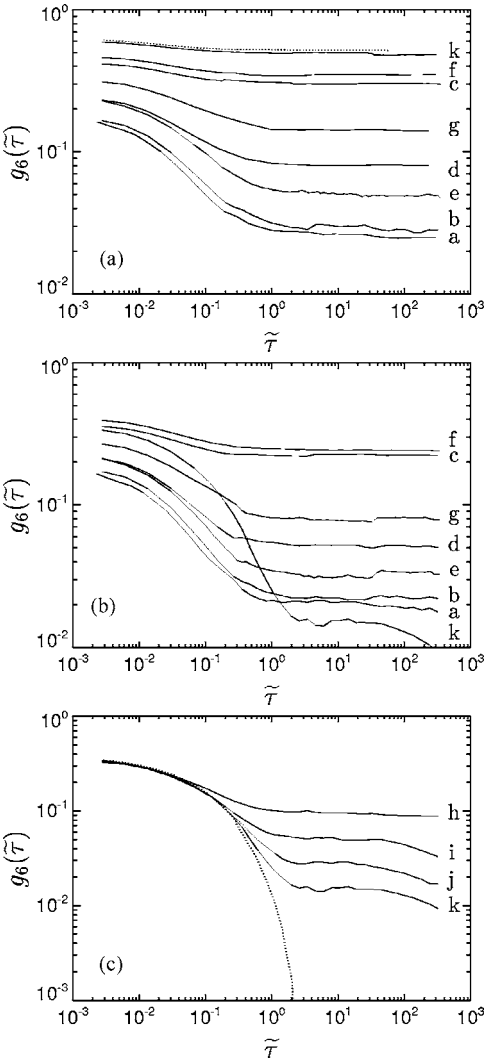

FIG. 2. The bulk bond-order correlation function at a dimensionless field strength of (a) $\Gamma = 16.13$, (b) $\Gamma = 12.41$ for a variety of channel widths. (c) The bulk bond-order correlation function at a dimensionless field strength of $\Gamma = 12.41$ for large channel widths. The letters a, b, c, d, e, f, g, h, i, j, and k correspond to the dimensionless channel widths 3, 3.12, 3.46, 4, 4.15, 4.62, 5, 10, 20, 50, and 100, respectively. The dotted line corresponds to the unbounded system at a dimensionless field strength of (a) $\Gamma = 16.13$ and (c) $\Gamma = 12.41$.

A. Local dynamics

The origin of the plateau is due to the presence of the parallel flat walls in the channel systems. The walls create a region of stable structure that extends away from the wall into the middle of the channel. We are interested in probing the local dynamics in these regions and therefore we chose to look at the bond-order correlation function in time for different sections of the channel. We analyzed $g_6(\tilde{\tau})$ for strips of dimensionless width 2 along the length of the channel located at increasing distances from the walls. Therefore, the strip labelled 0-2 indicates the sections of the channel that are within a dimensionless distance of 2 from either wall. In our analysis, only colloids that remained in a given strip for the duration of the lag time were considered. Additionally,

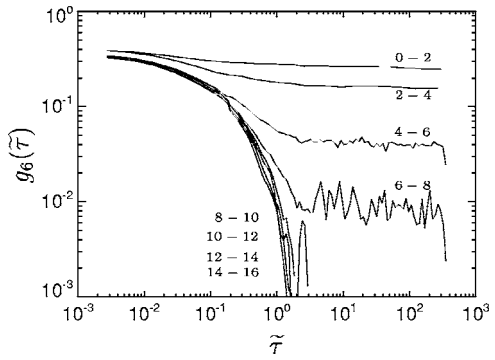

FIG. 3. The local bond-order correlation function at a dimensionless field strength $\Gamma=12.41$ and a dimensionless channel width $\tilde{w}=100$. The labels 0-2, 2-4, etc., refer to the dimensionless distance away from the wall where statistics were taken. The distances 8-10 through 14-16 away from the wall are statistically indistinguishable from one another and from the bond-order correlation function for the unbounded system at this field strength.

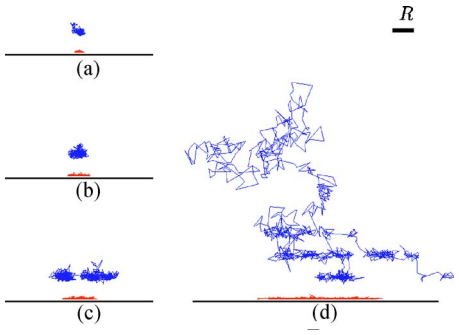

FIG. 4. (Color online) Trajectories for a bulk colloid (blue) and a neighboring wall colloid (red) over four different times at a dimensionless field strength of $\Gamma=12.41$ in a channel of dimensionless width $\tilde{w}=100$. The total trajectory time is (a) $\tilde{\tau}=0.373$, (b) $\tilde{\tau}=3.73$, (c) $\tilde{\tau}=37.3$, and (d) $\tilde{\tau}=373$. The channel wall is drawn as a solid line.

only bulk colloids were considered for this analysis (e.g., in the strip labelled 0-2, the colloids within a distance $R/2$ from the wall were not used in the analysis). The results of this analysis are shown in Fig. 3 for a dimensionless channel width of 100 at a dimensionless field strength of 12.41. In the regions nearest the wall (0-2 to 2-4) there is a very well defined plateau in $g_6(\tilde{\tau})$ over all dimensionless lag times. As we move farther away from the walls (4-6 to 6-8) there is still a distinguishable plateau in $g_6(\tilde{\tau})$ over all lag times but it is plagued by large statistical noise. The poor statistics are the result of the fact that the colloids in these sections do not remain in their respective sections for very long times. If we move even farther away from the wall (8-10 to 14-16) there is no longer a statistically distinguishable plateau in $g_6(\tilde{\tau})$ and all of the curves fall on top of the curve for the unbounded system at this dimensionless field strength. These results bring to light many interesting features of the dynamics in these systems. In the sections where there is a plateau in $g_6(\tilde{\tau})$, it remains constant until the longest lag time for which we have statistics. Additionally, the value of this plateau is continuously decreasing as we move away from the wall until there is no longer a statistically significant plateau. This continuous decrease indicates that there is no well defined boundary between the "wall" region and the "bulk" region but rather there is a continuous transition from one to the other. This result is similar to the observations made by Segalman *et al.* [33] for a system of block copolymers confined in two-dimensional channels. Teng *et al.* [31] also observed the decay of order as one moves away from the confining walls in a dusty plasma system. Additionally, in their results for $g_6(\tilde{\tau})$ they observed a plateau for the sections near the walls in good agreement with our results.

Now we address the issue of the subsequent decay in the plateau in large channels [Fig. 2(c)] since no such decay is observed within the sections nearest the wall in Fig. 3. The reason for the decay is actually related to the mobility of the colloids in the different regions of the channel. As mentioned previously, the statistics in Fig. 3 for the sections 4-6 and 6-8 away from the wall become rather poor at long times due to this mobility. In Fig. 4 we show trajectories for two colloids over four different dimensionless lag times in a dimensionless channel width of 100 at a dimensionless field strength of 12.41. For all of the lag times, the colloid against the wall remains very localized next to the wall but becomes increasingly mobile in the direction parallel to the wall. For a dimensionless lag time $\lesssim 1$ [Fig. 4(a)] the colloid in the bulk is able to explore its local region without feeling the constraint of its neighboring colloids. This type of behavior is seen uniformly over the entire width of the channel and gives rise to the initial exponential decay in the bond-order correlation function. Over intermediate lag times [Figs. 4(b) and 4(c)] that colloid completely explores its local environment but remains trapped in its local region near the wall. Since the colloid remains trapped in this local region its orientation with respect to its neighbors remains well correlated in time and therefore a plateau develops in $g_6(\tilde{\tau})$. Over very long lag times [Fig. 4(d)] the bulk colloid is able to escape the region near the wall and make an excursion into the center of the channel. This excursion causes the correlation of the bond-order for this colloid to decay and therefore the plateau in $g_6(\tilde{\tau})$ begins to decay for very long lag times.

Figures 3 and 4 illustrate that the structure in the different regions of the channel combined with the different dynamics in those regions give rise to the unusual behavior of the bond-order correlation function in time. The region closest to the wall is highly structured and the colloids there have low mobility while the regions far from the wall have less structure and high mobility. The exchange of colloids between these two regions of the channel is slow and therefore over intermediate times there is a plateau in $g_6(\tilde{\tau})$ before the colloids near the wall can escape into the bulk. It is important to note that in Fig. 2(c) the decay in the plateau is only seen for channels wider than ~ 20, matching well with what we have found in Fig. 3 where we observed a persistent plateau in $g_6(\tilde{\tau})$ out to a dimensionless distance of 8 from the walls. This means that, at this dimensionless field strength, in channels with a dimensionless width narrower than ~ 16 there are no regions where the $g_6(\tilde{\tau})$ curve decays to zero and therefore in these channels we would expect the plateau to persist for all lag times.

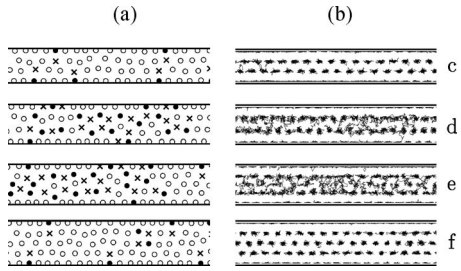

FIG. 5. (a) Snapshots of equilibrium defect configurations at a dimensionless field strength of $\Gamma=16.13$ for sections of dimensionless length 20, in four different channel widths c, d, e, and f corresponding to $\tilde{w}=3.46$, 4, 4.15, and 4.62, respectively (keeping consistent notation from the curves in Fig. 2). Open thin circles correspond to sixfold coordinated colloids (or fourfold if on a wall), closed circles correspond to fivefold coordinated colloids (or threefold if on a wall), × symbols correspond to sevenfold coordinated colloids (or fivefold if on a wall). (b) Trajectories of the colloids in that section of the channels for a time of $\tilde{\tau}=3.73$.

The behavior of the bond-order correlation function and the dynamics of the colloids in general are intimately related to the defects in these 2D systems [11,14]. We have observed that the channel-like confinement gives rise to some very interesting defect properties [35] and we will now discuss in more detail how those defect properties affect the dynamics of the colloids in 2D channels.

B. Link between structure and dynamics

It is well known that defects can give rise to increased mobility of the colloids in a solid 2D crystal. This point is illustrated for the channel systems in Fig. 5. Figure 5(a) shows the defect structure for four different dimensionless channel widths (3.46, 4, 4.15, and 4.62) at a dimensionless field strength of 16.13. In the channel systems, a bulk colloid is said to be a defect if it has more or less than six neighbors while a wall colloid is said to be a defect if it has more or less than four neighbors. It is quite evident that the defect concentration is larger for the intermediate channel widths of 4 and 4.15 than it is for the channel widths of 3.46 and 4.62. Additionally, it is important to note that even in the channels with a low concentration of defects (3.46 and 4.62) there are still regular dislocations along the wall [35]. Comparing the defect structures in Fig. 5(a) with the trajectories shown in Fig. 5(b) it is seen that the colloids in the channels with more defects are significantly more mobile than those in the channels with lower defect concentration. Similar to the trajectories in Fig. 4, the colloids along the wall remain highly localized even if there is significant mobility of the colloids in the bulk.

Again, the behavior (and the magnitude) of $g_6(\tilde{\tau})$ is highly correlated to the defect structure of the 2D system. Therefore comparing the curves in Fig. 2(a) for the same dimensionless channel widths as in Fig. 5 we see that the oscillations in the trend of $g_6(\tilde{\tau})$ as a function of channel width come about because of oscillations in the defect concentration. In the unbounded 2D system both the bond-order correlation function in time and information about the defects can be used to characterize the phase of the system and therefore we will apply a similar analysis to our 2D channel systems.

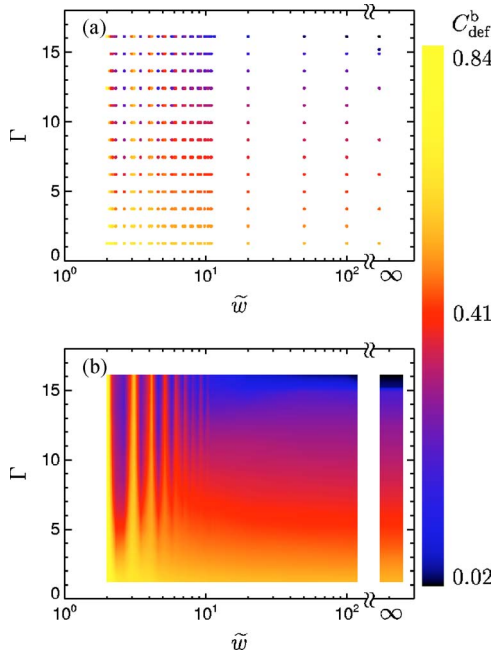

FIG. 6. (Color online) (a) Bulk defect concentration as a function of channel width and field strength. Light (yellow) indicates a high concentration of defects and dark (black) indicates a low concentration of defects. Each symbol designates a simulation result. (b) Continuum plot of bulk defect concentration as a function of channel width and field strength. Continuous contours have been interpolated along lines of constant defect concentration from the data in (a).

V. STATE-DIAGRAM OF A LATERALLY CONFINED DIPOLAR SYSTEM

As we have shown in Sec. IV A, the channel system is quite heterogeneous with the regions near the wall having different behavior than the regions farther away from the wall. Additionally, there is no well defined boundary between these two regions and therefore it is very difficult to define a "phase" for the entire channel system. We can however produce a map of the properties of the system as a function of the independent thermodynamic variables controlling the system (Γ and $\tilde{w}$). An example of this type of state diagram is shown in Fig. 6 where we have chosen to map the system property of bulk-defect concentration ($C^b_{\rm def}$) as it is closely related to the dynamics of the 2D channel system. The bulk-defect concentration is the fraction of colloids in the bulk that are defects. In Fig. 6(a) we show the value of the bulk-defect concentration for each set of conditions that we simulated. In Fig. 6(b) we show an interpolated continuous contour plot for the same data in order to more clearly illustrate the trends in the data. The most obvious characteristic of the state diagram in Fig. 6 is the re-entrant behavior observed as a function of dimensionless channel width. The periodicity of the oscillations in the bulk-defect concentration as a function of channel width is $\sim R$. This observation suggests that

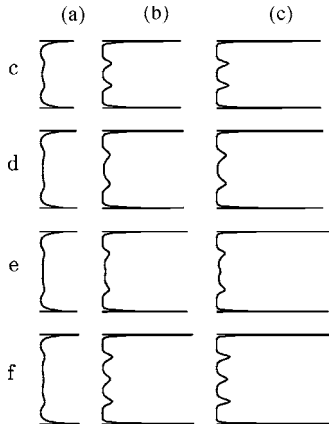

FIG. 7. Density profiles across the channels for three different dimensionless field strengths (a) $\Gamma=2.48$, (b) $\Gamma=8.69$, (c) $\Gamma=13.65$. Density profiles are given for four dimensionless channel widths c, d, e, and f corresponding to $\tilde{w}=3.46$, 4, 4.15, and 4.62, respectively (keeping consistent notation from the curves in Fig. 2).

the parallel channel walls cause a periodic destabilization of the crystal in the bulk as the channel width is decreased. We do not observe any re-entrant behavior as a function of dimensionless field strength, in contrast to systems confined in 2D circles or periodic 1D light fields [22,25,26,28–30].

A state-diagram such as this is important in that it shows how sensitive the structures, and therefore dynamics, in 2D channel systems are to the geometric constraints imposed upon the system. The state-diagram presented here is quite general and similar trends occur for other properties of the channel-like 2D system such as the local orientational order parameter (Ψ_6) and even the value of the plateau in $g_6(\tilde{\tau})$. Additionally, the re-entrant behavior as a function of the dimensionless channel width is an interesting characteristic that has not been observed in other 2D confining geometries.

As an example of the effect of Γ on the structure of the system we show density profiles for four different dimensionless channel widths in Fig. 7. The four dimensionless channel widths in Fig. 7 are the same as the four channels shown in Fig. 5. For all of the dimensionless field strengths in Fig. 7 there is a large magnitude peak in the density profiles occurring at the walls [35]. For low Γ systems [Fig. 7(a)] there is not a significant qualitative difference between the density profiles for the four channels. However, as Γ is increased [Figs. 7(b) and 7(c)] the density profiles for dimensionless channel widths 3.46 and 4.62 begin to appear strikingly different from the profiles for dimensionless channel widths 4 and 4.15. Sharp peaks in the density profiles appear for $\tilde{w}=3.46$ and 4.62 while for dimensionless channel widths of 4 and 4.15 the peaks are not as pronounced and there is less order across the channel.

VI. GENERALITY OF RE-ENTRANT BEHAVIOR FOR REPULSIVE POTENTIALS

We have compared our results for the dipolar system with two other systems described here. The first system consists of colloids interacting via a r^{-6} potential defined as

$$V_{6ij}(r_{ij}) = \epsilon_6\left(\frac{d}{r_{ij}}\right)^6. \tag{8}$$

Similar to the dipolar system, we define a dimensionless field strength Γ_6 as

$$\Gamma_6 = \frac{\epsilon_6}{k_B T}\left(\frac{d}{R}\right)^6, \tag{9}$$

where the length scale R is as defined for the dipolar system. The simulation details for the r^{-6} system are identical to those described in Sec. II for the dipolar system and $d \ll R$ so R is still the only important length scale.

The second system consists of hard-spheres confined in a 2D channel. The analogous term for the dimensionless field strength Γ_{HS} is defined for this system as [45]

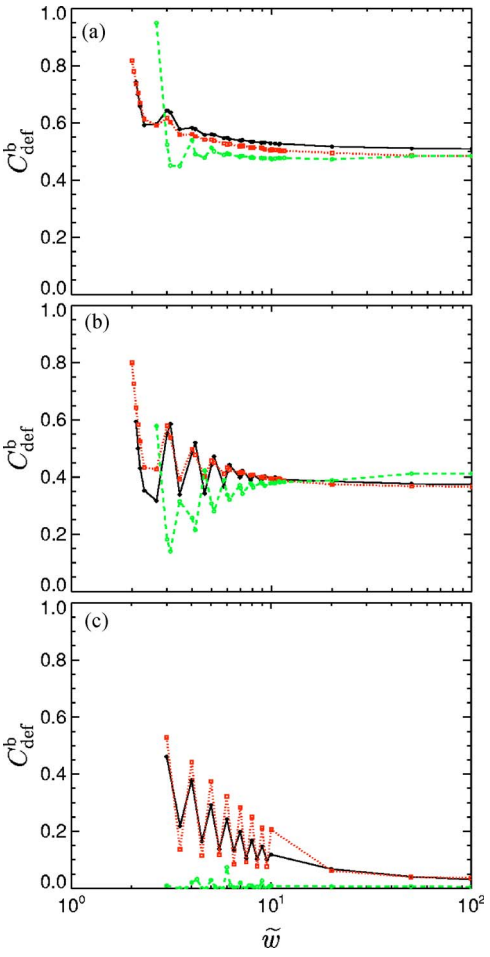

FIG. 8. (Color online) Concentration of defects in the bulk as a function of dimensionless channel width at three different dimensionless field strengths (a) $\Gamma=0.16\Gamma^*$, $\Gamma_6=0.16\Gamma^*_6$, $\Gamma_{HS}=0.79\Gamma^*_{HS}$ (unbounded liquid phase) (b) $\Gamma=0.58\Gamma^*$, $\Gamma_6=0.58\Gamma^*_6$, $\Gamma_{HS}=0.9\Gamma^*_{HS}$ (unbounded liquid phase) (c) $\Gamma=1.13\Gamma^*$, $\Gamma_6=1.13\Gamma^*_6$, $\Gamma_{HS}=1.13\Gamma^*_{HS}$ (unbounded solid phase). The (black) solid lines correspond to the dipolar system (r^{-3}), the (red) dotted lines correspond to the r^{-6} system, and the (green) dashed lines correspond to the hard sphere system.

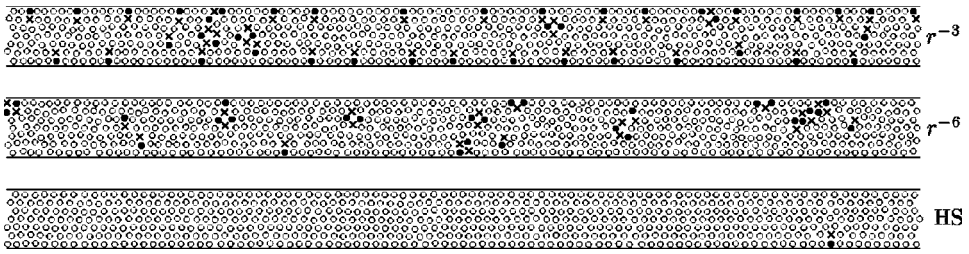

FIG. 9. Snapshots of equilibrium defect configurations in channels with a dimensionless width of $\tilde{w}=6.5$ and a dimensionless field strength of $\Gamma=1.13\Gamma^*$, $\Gamma_6=1.13\Gamma_6^*$, $\Gamma_{\mathrm{HS}}=1.13\Gamma_{\mathrm{HS}}^*$. Each snapshot shows a section of dimensionless length 100 (total dimensionless channel length is 170). Open thin circles correspond to sixfold coordinated colloids (or fourfold if on a wall), closed circles correspond to fivefold coordinated colloids (or threefold if on a wall), $\times$ symbols correspond to sevenfold coordinated colloids (or fivefold if on a wall). The channel walls are shown as solid lines.

$$\Gamma_{\mathrm{HS}} = nd^2, \tag{10}$$

where n is again the number density in the system. For the hard sphere system, the important length scale is now d so the dimensionless channel width for these systems is defined as the true width of the channel scaled by d. Additionally time is made dimensionless as $\tilde{t}=tk_BT/\zeta d^2$ for this system. The simulations of the hard sphere systems utilized the same dimensionless time step and total times as the dipole system. The algorithm developed by Heyes [40] was used to treat hard sphere interactions for this system.

Löwen [45] reports values for the solid-liquid phase transition for these two systems in the unbounded limit as $\Gamma_6^*=5.33$ and $\Gamma_{\mathrm{HS}}^*=0.887$ (where the asterisk refers to the phase transition point) giving us a reference for solid and liquid phases in these two systems. In Sec. III we showed that the phase transition in the dipolar system occurs in the range $\Gamma=14.89-15.2$ so for this section we will take $\Gamma^*=15.045$ for the dipolar system.

In Fig. 8 we illustrate the general result of re-entrant behavior in 2D channel systems by showing data for bulk defect concentration as a function of dimensionless channel width for the three different types of 2D colloidal systems. In Figs. 8(a) and 8(b) the dimensionless field strengths are such that the unbounded systems would be in the liquid phase while in Fig. 8(c) the dimensionless field strengths are large so that the unbounded systems would be well into the solid phase. The curves in Fig. 8 are equivalent to taking slices of constant Γ in Fig. 6. The hard sphere results in Figs. 8(a) and 8(b) were done for different fractions of Γ_{HS}^* than the respective simulations for the dipole and r^{-6} systems. This is because the hard sphere system becomes a gas if the number density is too low and therefore loses all structure. In Fig. 8, as the interaction strength is increased, it is evident that the re-entrant behavior of the bulk defect concentration as a function of channel width becomes more pronounced for the dipolar and r^{-6} systems. For the hard sphere curves in Figs. 8(a) and 8(b) this trend is evident as well. In Fig. 8(c) the Γ_{HS} for the hard sphere system is large enough that there are hardly any defects in any of the channel widths but even this system still exhibits re-entrant behavior as a function of channel width. These results strongly suggest that the general form of the state-diagram shown in Fig. 6 holds for 2D colloidal systems confined in hard-wall channels and interacting with repulsive potentials.

There are significant differences, however, between the three different types of colloidal systems. For instance, in Fig. 8(c) the hard sphere system is nearly perfect due to the high number density while the other two systems still exhibit significant defect concentrations. A qualitative example of this difference between the systems is given in Fig. 9 where we present snapshots of the defect structure in a section of a channel with dimensionless width 6.5 for the three different systems. The dimensionless field strengths in Fig. 9 are $\Gamma=1.13\Gamma^*$, $\Gamma_6=1.13\Gamma_6^*$, and $\Gamma_{\mathrm{HS}}=1.13\Gamma_{\mathrm{HS}}^*$, all well into the solid phase for the unbounded systems. It is evident that the three systems have significantly different defect distributions. The dipolar system shows the regular dislocations along the wall that have been reported previously [35], while the other two systems exhibit no such regular defects along the walls. Rather, in the r^{-6} system, the defects are found in small clusters that are distributed along the length of the channel. In the hard sphere system there are very few, short lived, pairs of dislocations showing evidence of the extreme ordering mentioned above.

VII. DISCUSSION AND CONCLUSIONS

An analysis has been presented of the structure and dynamics in a system of repulsive dipoles confined in 2D channels. We have compared the dynamical properties of these systems to the case of an unbounded 2D system. We have performed careful simulations of the unbounded system in an attempt to determine over which range of dimensionless field strengths the solid-liquid phase transition occurs. We were able to determine that the phase transition occurs in a narrow range of dimensionless field strengths (between 14.89 and 15.2) but we were unable to converge our simulations of the unbounded system between these two dimensionless field strengths. Experimentally, a hexatic phase has been observed in this system [13–15] indicating that it may be possible to observe this type of phase in a simulation with an extremely large number of colloids.

We perturbed this 2D unbounded system by introducing parallel hard walls to create a channel-like geometry. In the channel systems we observed dynamics that differed significantly from the unbounded system. We observed the exis-

tence of a plateau in the bond-order correlation function due to the stabilizing presence of a hard wall. We also observed that the channel systems exhibited strikingly different local structure and dynamics in the regions near the wall and farther away from the walls causing both the onset and the subsequent decay of the plateau in the bond-order correlation function in large channels at lower dimensionless field strengths. The heterogeneity of the channel systems was shown by calculating the bond-order correlation function in different sections of the channel. We observed a decay in the correlation function as we moved away from the walls in our channel systems. This observation is consistent with studies performed on spherical block copolymers confined in very wide 2D channels [33]. However, combining this observation with our analysis of the local dynamics of the colloids leads to an explanation of the anomalous form of the $g_6(\bar{\tau})$ curves seen in this 2D channel system.

The dynamics in 2D colloidal systems are strongly linked to the defect properties of those systems and we showed this to be true for the 2D channel systems as well. We have presented a state-diagram for dipoles confined in a 2D channel system as a function of dimensionless field strength and dimensionless channel width that summarizes the behavior of these systems. The qualitative aspects of the state-diagram are applicable to any order parameter of the 2D channel system as they are all linked to the structure and dynamics. Additionally, by simulating systems with sharper repulsive potentials we have shown that the general form of the state-diagram presented here (with re-entrant behavior) can be considered universal for colloids in 2D hard-wall channels interacting with repulsive potentials.

We have observed re-entrant behavior in the properties of the dipolar system as a function of the geometry of the system, not the dimensionless field strength. This finding is similar to the re-entrant behavior observed in other simulation studies of colloids confined in 2D channels [34] demonstrating that, qualitatively, this behavior can be seen for a variety of colloidal interactions as well as confining potentials. Despite the qualitative similarities however, there are important differences between the hard wall confinement presented here and the parabolic confinement studied previously. These differences have been discussed extensively in the case of 2D circular geometries [25–27,46]. An important distinction between these two types of confinement is that the systems with parabolic confinement have a homogeneous distribution of colloids while the hard wall confinement leads to an inhomogeneous distribution throughout the system due to the high density of colloids along the walls. This higher density along the walls was observed in the case of channel-like confinement as well [35]. Another important difference between these two types of confinement is that the average density of colloids remains constant when the external field strength is decreased in hard wall systems while in systems with parabolic confinement the average density of colloids increases with decreased external field strength. As a result of these two very important distinctions, hard wall systems and parabolic systems can behave quite differently, even in the case of channels. An example of this difference in behavior is the unusual structural transition from four rows to three rows and then back to four rows as the interaction strength between colloids was increased in parabolic channel-like confinement [34]. No such structural transition is observed in the case of hard wall confinement. However, as mentioned previously, both systems do exhibit re-entrant behavior.

We did not observe any re-entrant behavior as a function of dimensionless field strength but the re-entrant behavior as a function of the dimensionless channel width implies that the structural properties and therefore the dynamics of these self-assembled colloidal systems in microfluidic geometries are very sensitive to the confinement geometry itself. This will have an impact upon many applications where both the structure and mobility of the self-assembled colloids are important considerations in the application design.

ACKNOWLEDGMENTS

We gratefully acknowledge the support of NSF NIRT Grant No. CTS-0304128 for this project. We would also like to thank Markus Hüetter for his input and advice.

[1] J. Liu, E. M. Lawrence, A. Wu, M. L. Ivey, G. A. Flores, K. Javier, J. Bibette, and J. Richard, Phys. Rev. Lett. **74**, 2828 (1995).
[2] P. Carletto and G. Bossis, J. Phys.: Condens. Matter **15**, S1437 (2003).
[3] T. Ukai and T. Maekawa, Phys. Rev. E **69**, 032501 (2004).
[4] P. S. Doyle, J. Bibette, A. Bancaud, and J.-L. Viovy, Science **295**, 2237 (2002).
[5] N. Minc, C. Fütterer, K. D. Dorfman, A. Bancaud, C. Gosse, C. Goubault, and J.-L. Viovy, Anal. Chem. **76**, 3770 (2004).
[6] M. A. Hayes, N. A. Polson, and A. A. Garcia, Langmuir **17**, 2866 (2001).
[7] M. A. Hayes, N. A. Polson, A. N. Phayre, and A. A. Garcia, Anal. Chem. **73**, 5896 (2001).
[8] A. Rida and M. A. M. Gijs, Appl. Phys. Lett. **85**, 4986 (2004).
[9] A. Rida and M. A. M. Gijs, Anal. Chem. **76**, 6239 (2004).
[10] J. Kosterlitz and J. Thouless, J. Phys. C **6**, 1181 (1973).
[11] B. I. Halperin and D. R. Nelson, Phys. Rev. Lett. **41**, 121 (1978).
[12] A. P. Young, Phys. Rev. B **19**, 1855 (1979).
[13] K. Zahn and G. Maret, Phys. Rev. Lett. **85**, 3656 (2000).
[14] K. Zahn, R. Lenke, and G. Maret, Phys. Rev. Lett. **82**, 2721 (1999).
[15] R. E. Kusner, J. A. Mann, J. Kerins, and A. J. Dahm, Phys. Rev. Lett. **73**, 3113 (1994).
[16] P. S. Branício, J.-P. Rino, and N. Studart, Phys. Rev. B **64**, 193413 (2001).
[17] K. Binder, S. Sengupta, and P. Nielaba, J. Phys.: Condens. Matter **14**, 2323 (2002).
[18] A. Jaster, Phys. Rev. E **59**, 2594 (1999).
[19] K. Bagchi, H. C. Andersen, and W. Swope, Phys. Rev. Lett. **76**, 255 (1996).

[20] H. Watanabe, S. Yukawa, Y. Ozeki, and N. Ito, Phys. Rev. E **69**, 045103(R) (2004).
[21] T. Terao and T. Nakayama, Phys. Rev. E **60**, 7157 (1999).
[22] R. Bubeck, C. Bechinger, S. Neser, and P. Leiderer, Phys. Rev. Lett. **82**, 3364 (1999).
[23] Y.-J. Lai and L. I, Phys. Rev. E **64**, 015601(R) (2001).
[24] M. Kong, B. Partoens, and F. M. Peeters, Phys. Rev. E **67**, 021608 (2003).
[25] I. V. Schweigert, V. A. Schweigert, and F. M. Peeters, Phys. Rev. Lett. **84**, 4381 (2000).
[26] R. Bubeck, P. Leiderer, and C. Bechinger, Prog. Colloid Polym. Sci. **118**, 73 (2001).
[27] M. Kong, B. Partoens, A. Matulis, and F. M. Peeters, Phys. Rev. E **69**, 036412 (2004).
[28] J. Chakrabarti, H. R. Krishnamurthy, A. K. Sood, and S. Sengupta, Phys. Rev. Lett. **75**, 2232 (1995).
[29] Q.-H. Wei, C. Bechinger, D. Rudhardt, and P. Leiderer, Phys. Rev. Lett. **81**, 2606 (1998).
[30] E. Frey, D. R. Nelson, and L. Radzihovsky, Phys. Rev. Lett. **83**, 2977 (1999).
[31] L.-W. Teng, P.-S. Tu and L. I, Phys. Rev. Lett. **90**, 245004 (2003).
[32] R. A. Segalman, A. Hexemer, and E. J. Kramer, Macromolecules **36**, 6831 (2003).
[33] R. A. Segalman, A. Hexemer, and E. J. Kramer, Phys. Rev. Lett. **91**, 196101 (2003).
[34] G. Piacente, I. V. Schweigert, J. J. Betouras, and F. M. Peeters, Phys. Rev. B **69**, 045324 (2004).
[35] R. Haghgooie and P. S. Doyle, Phys. Rev. E **70**, 061408 (2004).
[36] R. Pesché, M. Kollmann, and G. Nägele, Phys. Rev. E **64**, 052401 (2001).
[37] K. Zahn, J. M. Méndez-Alcaraz, and G. Maret, Phys. Rev. Lett. **79**, 175 (1997).
[38] H. Zhang and M. Widom, Phys. Rev. E **51**, 2099 (1995).
[39] H. C. Öttinger, *Stochastic Processes in Polymeric Fluids: Tools and Examples for Developing Simulation Algorithms* (Springer, Berlin, 1996).
[40] D. Heyes and J. Melrose, J. Non-Newtonian Fluid Mech. **46**, 1 (1993).
[41] D. Frenkel and B. Smit, *Understanding Molecular Simulation from Algorithms to Applications*, 2nd ed. (MPG Books, Bodmin, Great Britain, 2002).
[42] C. Reichhardt and C. Olson Reichhardt, Phys. Rev. Lett. **90**, 095504 (2003).
[43] D. Nelson, *Phase Transitions and Critical Phenomena*, edited by C. Domb and J. L. Lebowitz (Academic, London, 1983).
[44] K. J. Strandburg, Rev. Mod. Phys. **60**, 161 (1988).
[45] H. Löwen, Phys. Rev. E **53**, R29 (1996).
[46] V. M. Bedanov and F. M. Peeters, Phys. Rev. B **49**, 2667 (1994).